

# Synoptic Moisture Intrusion Provided Heavy Isotope Precipitations in Inland Antarctica during the Last Glacial Maximum

Kanon Kino<sup>1</sup>, Alexandre Cauquoin<sup>2</sup>, Atsushi Okazaki<sup>3,4</sup>, Taikan Oki<sup>5</sup>, and Kei Yoshimura<sup>2</sup>

<sup>1</sup>The University of Tokyo

<sup>2</sup>Institute of Industrial Science, The University of Tokyo

<sup>3</sup>Hirosaki University

<sup>4</sup>Chiba University

<sup>5</sup>University of Tokyo

April 16, 2024

## Abstract

Stable water isotopes in inland Antarctic ice cores are powerful paleoclimate proxies; however, their relationship with dynamical atmospheric circulations remains controversial. Using a water isotope climate model (MIROC5-iso), we assessed the influence of the Last Glacial Maximum (LGM; ~21,000 years ago) sea surface temperatures (SST) and sea ice (SIC) on Antarctic precipitation isotopes ( $\delta^{18}\text{O}_p$ ) through atmospheric circulation. The results revealed that the synoptic circulation mostly maintained southward moisture transport, reaching inland Antarctica. The steepened meridional SST gradient in the mid-latitudes increased  $\delta^{18}\text{O}_p$  in inland Antarctica by enhancing the baroclinic instability and synoptic moisture transport. In contrast, enhanced SIC reduced the atmospheric humidity around Antarctica and lowered  $\delta^{18}\text{O}_p$  through extensive surface cooling and transport from the ocean. These findings elucidate the isotopic proxies and enable us to constrain the southern hemisphere atmospheric circulation, including the westerlies, using ice cores during past climates, including the LGM.

## Hosted file

983913\_0\_supp\_11747445\_s6shcq.docx available at <https://authorea.com/users/588705/articles/699418-synoptic-moisture-intrusion-provided-heavy-isotope-precipitations-in-inland-antarctica-during-the-last-glacial-maximum>

1                   **Synoptic Moisture Intrusion Provided Heavy Isotope Precipitations in**  
2                   **Inland Antarctica during the Last Glacial Maximum**

3  
4 **K. Kino<sup>1</sup>, A. Cauquoin<sup>2</sup>, A. Okazaki<sup>3</sup>, T. Oki<sup>1</sup>, and K. Yoshimura<sup>2</sup>**

5  
6 <sup>1</sup>Department of Civil Engineering, Graduate School of Engineering, the University of Tokyo,  
7 Tokyo, Japan

8 <sup>2</sup>Institute of Industrial Science, the University of Tokyo, Kashiwa, Japan

9 <sup>3</sup>Chiba University, Chiba, Japan

10 Corresponding author: Kanon Kino (kanon@hydra.t.u-tokyo.ac.jp)

11  
12  
13 **Key Points:**

- 14       • Synoptic circulations sustained the moisture transport toward inland Antarctica.  
15       • Meridional sea surface temperature gradient enhanced moisture and heavy isotope  
16       precipitations on Antarctica, unlike sea ice expansion.  
17       • Antarctic ice core isotopes may refine southern westerlies during the last glacial  
18       maximum.

19

20

## 21 Abstract

22 Stable water isotopes in inland Antarctic ice cores are powerful paleoclimate proxies; however,  
23 their relationship with dynamical atmospheric circulations remains controversial. Using a water  
24 isotope climate model (MIROC5-iso), we assessed the influence of the Last Glacial Maximum  
25 (LGM; ~21,000 years ago) sea surface temperatures (SST) and sea ice (SIC) on Antarctic  
26 precipitation isotopes ( $\delta^{18}\text{O}_p$ ) through atmospheric circulation. The results revealed that the  
27 synoptic circulation mostly maintained southward moisture transport, reaching inland Antarctica.  
28 The steepened meridional SST gradient in the mid-latitudes increased  $\delta^{18}\text{O}_p$  in inland Antarctica  
29 by enhancing the baroclinic instability and synoptic moisture transport. In contrast, enhanced  
30 SIC reduced the atmospheric humidity around Antarctica and lowered  $\delta^{18}\text{O}_p$  through extensive  
31 surface cooling and transport from the ocean. These findings elucidate the isotopic proxies and  
32 enable us to constrain the southern hemisphere atmospheric circulation, including the westerlies,  
33 using ice cores during past climates, including the LGM.

## 34 Plain Language Summary

35 Stable water isotopes are widely used to reconstruct past variations of Earth's climate, such as  
36 the temperature in Antarctica during the Last Glacial Maximum (LGM) ~21,000 years ago. This  
37 is an essential period for the climate community, given the order of magnitude of the temperature  
38 change between the LGM and today, which is similar to that of today's warming. However, the  
39 relationship between stable water isotopes and temperature is still subject to debate because of  
40 the influence of other climatic factors. Using an isotope-enabled climate model, we found that  
41 the isotopic composition of Antarctic precipitation was not simply controlled by condensation  
42 temperature, but was substantially influenced by changes in dynamical atmospheric circulation  
43 related to sea surface temperature and sea ice expansion. We also suggest that representation of  
44 the past atmospheric circulations, including westerly jets, can be constrained using water isotopic  
45 signals in Antarctic ice cores.

## 46 1 Introduction

47 Ratios of stable isotopologues of water,  $\text{H}_2^{16}\text{O}$ ,  $\text{H}_2^{18}\text{O}$ , and  $\text{HD}^{16}\text{O}$ , expressed hereafter in  
48 the usual  $\delta$  notation (i.e.,  $\delta^{18}\text{O}$ , with respect to V-SMOW scale; Dansgaard, 1964), from  
49 Antarctic ice cores have been widely used to study Earth's climate variations for the past several  
50 hundred thousand years. For example, the obtained  $\delta^{18}\text{O}$  values allowed for describing the  
51 glacial-interglacial cycles over the past ~800,000 years (Augustin et al., 2004; Kawamura et al.,  
52 2017). The isotopic thermometer assumption, which regards the observed present-day spatial  
53  $T_a/\delta^{18}\text{O}$  slope as a surrogate for the temporal slope at a given site, has been classically used to  
54 reconstruct the mean surface air temperature changes ( $\Delta T_a$ ;  $\Delta$  denotes changes between  
55 climates) in the past (Dahe et al., 1994; Dansgaard, 1964; Lorius et al., 1979; Lorius & Merlivat,  
56 1977; Motoyama, 2005; Satow et al., 1999). Process-based reconstruction of the past Antarctic  
57  $T_a$  was also carried out using simple one-dimensional Lagrangian isotope models or water  
58 isotope-enabled climate models (iso-GCMs). Still, there are considerable uncertainties in our  
59 understanding of the global and Antarctic climate and associated isotope changes during the last  
60 glacial maximum (LGM): an extremely cold climate period characterized by a low atmospheric  
61  $\text{CO}_2$  level (approximately 180 ppm) and highly extended ice-sheets in the northern hemisphere  
62 (NH) (Kageyama, Abe-Ouchi, et al., 2021). As for the global climate, the degree of global mean  
63 cooling (Kageyama, Harrison, et al., 2021), spatial sea surface conditions (Paul et al., 2021),

64 state of the ocean general circulation (Sherriff-Tadano & Klockmann, 2021), and the ice-sheet  
65 topographies (Ivanovic et al., 2016) are the major remaining issues. As for the processes  
66 determining  $\delta^{18}\text{O}$  precipitation ( $\delta^{18}\text{O}_p$ ) in Antarctica, the moisture origin (Uemura et al., 2018),  
67 sea ice extension (Lee et al., 2008), ice-sheet topography (Werner et al., 2018), surface inversion  
68 layer depth (Buizert et al., 2021), and precipitation seasonality (Erb et al., 2018) possibly affect  
69 the temporal  $T_a/\delta^{18}\text{O}$  slope.

70 The role of atmospheric circulations in these processes has not been fully explored for  
71 past climates such as LGM despite extensive research. In modern Antarctica, several studies  
72 have indicated that dynamical circulations can influence  $\delta^{18}\text{O}_p$  and temporal  $T_a/\delta^{18}\text{O}_p$  slope  
73 (Dittmann et al., 2016; Fujita & Abe, 2006; Hirasawa et al., 2000, 2013; Kino et al., 2021;  
74 Noone & Simmonds, 2002; Schlosser et al., 2010, 2017; Stenni et al., 2016). Recent studies have  
75 also revealed the impacts of extreme precipitation events (EPE) on  $\delta^{18}\text{O}_p$  in Antarctica (Dittmann  
76 et al., 2016; Kino et al., 2021; Schlosser et al., 2017; Servettaz et al., 2020). Typical EPEs,  
77 associated with synoptic circulations (including blocking events and atmospheric rivers),  
78 facilitate the intrusion of warm and humid air into Antarctica (Fujita & Abe, 2006; Hirasawa et  
79 al., 2000, 2013; Turner et al., 2019; Wang et al., 2023; Wille et al., 2021). Low-frequency (intra-  
80 to inter-seasonal) atmospheric variabilities, such as the Southern Annular Mode (SAM), also  
81 influence precipitation amounts (Marshall et al., 2017) and  $\delta^{18}\text{O}_p$  in inland Antarctica (Kino et  
82 al., 2021). Such dynamical circulations could introduce bias to the  $\delta^{18}\text{O}$  in Antarctic ice cores  
83 ( $\delta^{18}\text{O}_{\text{ice}}$ ) as these ice cores are expected to reflect precipitation-weighted  $\delta^{18}\text{O}_p$  (Krinner &  
84 Werner, 2003; Sime & Wolff, 2011; Werner et al., 2018). Southern mid-latitude atmospheric  
85 circulations, including the southern westerlies, are linked with sea surface temperature (SST) and  
86 sea ice concentration (SIC) in the mid-latitudes for both the present-day (Nakamura et al., 2008)  
87 and LGM (Sime et al., 2013) climates. Given the uncertainties of SST and SIC (Paul et al., 2021)  
88 and the southern westerlies (Kohfeld et al., 2013; Sime et al., 2013) during LGM, understanding  
89 key processes that change Antarctic  $\delta^{18}\text{O}_p$  related to atmospheric circulations through a series of  
90 experiments for probable LGM conditions, is imperative.

91 In this study, the influence of southern mid-latitude atmospheric circulations on  $\delta^{18}\text{O}_p$  in  
92 Antarctica during the past climate, namely LGM, was investigated in relation to SST and SIC.  
93 We applied two recent sea surface reconstructions (Paul et al., 2021; Sherriff-Tadano et al.,  
94 2023) as boundary conditions for an isotope-enabled atmospheric GCM (iso-AGCM). This  
95 approach allowed us to comprehensively investigate the influence of atmospheric circulation on  
96 the Antarctic  $\delta^{18}\text{O}_p$ . The remainder of this paper is organized as follows. In Section 2, the model,  
97 experimental settings, observational dataset, and analysis method are discussed. In Section 3, we  
98 evaluate the simulated LGM climates in Antarctica and analyze the processes ruling the  $\delta^{18}\text{O}_p$  in  
99 Antarctica by investigating the differences between the simulated LGM experiments. In Section  
100 4, we summarize our main findings concerning the combined effects of SST and SIC on  $\delta^{18}\text{O}_p$   
101 and discuss issues that need to be resolved.

## 102 **2 Materials and Methods**

### 103 **2.1 Isotope-enabled atmospheric general circulation model**

104 The atmospheric component of the fifth version of the Model for Interdisciplinary  
105 Research on Climate (MIROC; Watanabe et al., 2010) is based on a three-dimensional primitive  
106 equation in the hybrid  $\sigma$ - $p$  coordinate, with spectral truncation adopted for horizontal  
107 discretization. Version MIROC5-iso, where water isotopes in the atmosphere and land surface

108 parts were implemented by Okazaki and Yoshimura (2017, 2019), was used in this study. The  
 109 resolution of the MIROC5-iso was set to a horizontal spectral truncation of T42 (approximately  
 110 280 km) and 40 vertical layers. Okazaki and Yoshimura (2017, 2019) and Kino et al. (2021)  
 111 discuss the detailed parameterizations of the models and their applications for global and  
 112 Antarctic present-day conditions.

113

## 114 2.2 Experimental design

115 Four experiments were performed using MIROC5-iso (Table 1). A pre-industrial (PI)  
 116 simulation was set up following the “piControl” experimental design in the Coupled Model  
 117 Intercomparison Project-Phase 6 (CMIP6; Eyring et al., 2016). The mean SST and SIC fields  
 118 (monthly averaged from 1870 to 1899) were obtained from the Atmospheric Modeling  
 119 Intercomparison Project-Phase 2 (AMIP2; Taylor et al., 2000). Three LGM experiments were  
 120 designed using the PMIP4 protocol (Kageyama et al., 2017). For the elevation and distribution of  
 121 the ice-sheet, the GLAC-1D reconstruction at year 21 ka (Briggs et al., 2014; Ivanovic et al.,  
 122 2016; Tarasov et al., 2012) was used. The land-sea mask was extended according to the ice-  
 123 sheet. The boundary conditions of the land surface were the same as those in the PI simulation  
 124 but masked by the LGM ice-sheet. The  $\delta^{18}\text{O}$  of seawater was set to a globally uniform value  
 125 (+1 ‰), according to Werner et al. (2018).

126

127 **Table 1** Experimental designs in this study. NH and SH indicate the northern and southern hemispheres. M  
 128 and G denote SIC provided by MIROC4m-AOGCM (Sherriff-Tadano et al., 2023) and GLOMAP (Paul et al.,  
 129 2021), respectively.

Experimental name	Greenhouse gases & orbital parameters	Land surfaces		Ocean surfaces			
		Ice sheets & land-sea mask	others	SST	SIC in NH	SIC in SH	$\delta^{18}\text{O}_{\text{sea water}}$ [‰]
PI	PI	PI	PI	PI	PI	PI	0
LGM_G	LGM	LGM	PI	G	G	G	+1
LGM_M	LGM	LGM	PI	M	M	M	+1
LGM_Mw/Gice	LGM	LGM	PI	M	M	G	+1

130

131 The LGM simulations differ in the prescribed SST and SIC to force MIROC5-iso. Two  
 132 recent sets were used to investigate the influence of sea surface conditions on LGM  $\delta^{18}\text{O}_p$  in  
 133 Antarctica. For LGM\_G, the monthly SST and SIC provided by the Glacial Ocean MAP  
 134 (GLOMAP; Paul et al., 2021) were used (Figure S1a). GLOMAP is a gridded LGM climatology  
 135 reconstruction dataset based on faunal and floral assemblage data of the Multiproxy Approach  
 136 for the Reconstruction of the Glacial Ocean Surface project and several estimates of the LGM  
 137 SIC. GLOMAP exhibits higher cooling in the Southern Ocean (SO) than another reconstruction,  
 138 as well as more extended SIC in this area. For LGM\_M, SST and SIC simulated by Sherriff-  
 139 Tadano et al. (2023; hereafter referred to as MIROC) were used (Figure S1b). The fourth  
 140 generation of MIROC atmosphere-ocean GCM simulated the weak Atlantic meridional  
 141 overturning circulation during LGM suggested by proxies, resulting in warmer LGM SST in the  
 142 SO than in the other models (Sherriff-Tadano et al., 2023). Sherriff-Tadano et al. (2023) further  
 143 improved expressions of mixed-phased clouds and reduced surface warm biases in the SO.  
 144 Detailed setup of MIROC5-iso simulations are presented in Text S1.

145 The sensitivity experiment, LGM\_Mw/Gice (i.e., MIROC SST and GLOMAP SIC), was  
 146 conducted to determine the effects of SST and SIC that differed from those of LGM\_G and  
 147 LGM\_M. Therefore, LGM\_G minus LGM\_Mw/Gice (LGM\_Mw/Gice minus LGM\_M)  
 148 indicates the individual influence of changes in SST (SIC). The SST and SIC changes between  
 149 LGM experiments are shown in Figures 1a–b and 2e–f.

150

### 151 2.3 Proxy data for model evaluation

152 Ten Antarctic ice core records were used for evaluation. For EDML, Dome B, Vostok,  
 153 Dome C, Taylor Dome, Talos, WDC, and Byrd,  $\Delta\delta^{18}\text{O}_{\text{ice}}$  and  $\Delta T_a$  for LGM minus PI in LGM  
 154 compiled by Werner et al. (2018) was employed. For  $\Delta\delta^{18}\text{O}$  of the South Pole, we used the  
 155 results of Steig et al. (2021). Each site location is shown in Figure 2a.

156  $\Delta\delta^{18}\text{O}$  data from speleothems (Comas-Bru et al., 2019; 2020) and ice cores (Kawamura et  
 157 al., 2007; Landais et al., 2013; Uemura et al., 2018) were used to evaluate the simulated LGM  
 158 climates at the global scale. For speleothems,  $\Delta\delta^{18}\text{O}$  in the calcite was obtained from the  
 159 Speleothem Isotope Synthesis and Analysis version 2 (SISALv2) dataset (Comas-Bru et al.,  
 160 2019). The speleothem values of  $\Delta\delta^{18}\text{O}$  were converted in drip water as performed by Cauquoin  
 161 et al. (2019), using the respective experiments and method outlined by Tremaine et al. (2011).

162

### 163 2.4 Analysis method

164 To investigate the impact of atmospheric variations across multiple timescales on  
 165 moisture transport to Antarctica, we decoupled the contributions of synoptic (associated with  
 166 EPEs), intra- to inter-seasonal (e.g., SAM), and climatological scale meridional moisture  
 167 transports by following Newman et al. (2012). First, the climatological mean state was  
 168 determined from daily time-series. The residuals of daily time-series anomalous from the daily  
 169 climatology were further decoupled to low-frequency and synoptic. The low frequency was  
 170 determined using a Lanczos low-pass filter, which passes periods greater than 10-day, and the  
 171 residual represented periods less than 10-day (synoptic state) using the SciPy library. Such  
 172 filtering methods were used for specific humidity ( $q$ ) and meridional wind speed ( $v$ ) in the model  
 173 vertical layers. We finally obtained the vertically integrated moisture transport ( $Q$ ) in each time  
 174 scale as follows:

$$175 \quad Q_m = \int_{p_s}^0 \overline{p_s v_m q_m} dp/g,$$

$$176 \quad Q_{LF} = \int_{p_s}^0 \overline{p_s v_{LF} q_{LF}} dp/g, \text{ and}$$

$$177 \quad Q_{syn} = \int_{p_s}^0 \overline{p_s v_{syn} q_{syn}} dp/g.$$

178 Here,  $p_s$  is the surface pressure, and  $g$  is the gravity constant. The overbar represents the time  
 179 mean, and the subscripts  $m$ ,  $LF$ , and  $syn$  are the climatological mean, the low frequency, and the  
 180 synoptic time scales, respectively.

181 **3 Results**

## 182 3.1 Evaluation of Last Glacial Maximum climate simulations in MIROC5-iso

183 By globally assessing the simulated  $\delta^{18}\text{O}_p$  reduction from PI to LGM, we confirmed that  
 184 MIROC5-iso reasonably reproduced the LGM climate with a root mean square error (RMSE) of  
 185  $\sim 3.1\%$  between the modeled and observed  $\Delta\delta^{18}\text{O}_p$  values (Figures S2b and S3b). Both LGM  
 186 simulations showed polar amplification in NH and SH, as well as global surface cooling, which  
 187 is consistent with previous studies ([Cauquoin et al., 2023](#); [Risi et al., 2010](#)). The reproducibility  
 188 in the mid-high and low latitudes varies based on the SST/SIC boundary conditions. The positive  
 189  $\Delta\delta^{18}\text{O}_p$  in the tropics ( $+1\text{--}2\%$ ) was significant in LGM\_G simulation, resulting in a more  
 190 optimized model-data agreement for tropical speleothems than in LGM\_M simulation (Figures  
 191 S2a and S3a).

192 For Antarctica, LGM\_G and LGM\_M results were reasonable compared to  $\Delta\delta^{18}\text{O}_{\text{ice}}$   
 193 (Figure S4a).  $\Delta\delta^{18}\text{O}_p$  in LGM\_G and LGM\_M exhibit different spatial distributions (Figures 2a–  
 194 b). In the simulations, the respective  $\Delta\delta^{18}\text{O}_p$  values of LGM\_G and LGM\_M were similar at  
 195 Dome Fuji, South Pole, and Dome B and consistent with the  $\Delta\delta^{18}\text{O}_{\text{ice}}$  at Dome Fuji and Dome B.  
 196 The  $\delta^{18}\text{O}$  reduction at South Pole was very underestimated in both LGM simulations, possibly  
 197 because of the unrealistic reduction of mean precipitation related to the precipitation amount  
 198 weighting effect on  $\delta^{18}\text{O}_p$ . The precipitation reduction from PI to LGMs was more at  
 199 approximately  $180^\circ$  and less at  $0^\circ$  longitude (Figure S5). Such spatial distribution would be  
 200 changed by the topography or local circulation. The LGM\_M results were relatively more  
 201 consistent with the  $\Delta\delta^{18}\text{O}_{\text{ice}}$  than the LGM\_G ones at EDML, Vostok, and Dome C, whereas  
 202 LGM\_G simulation overestimated the reduction for  $\sim 2\%$  in these sites. In contrast, LGM\_G  
 203 values were in good agreement with the observed  $\Delta\delta^{18}\text{O}_{\text{ice}}$  at WDC and Byrd, whereas LGM\_M  
 204 experiment underestimated the  $\delta^{18}\text{O}$  reduction by  $\sim 3\%$  in these sites. To resume, MIROC5-iso  
 205 LGM\_G and LGM\_M simulations were generally in better agreement with isotopic observation  
 206 in West and East Antarctica, respectively. For certain ice core sites, our  $\Delta\delta^{18}\text{O}_p$  results differ  
 207 from those of the LGM experiments by Cauquoin et al. (2023) carried out with ECHAM6-wiso.  
 208 For example, the decrease in  $\delta^{18}\text{O}_p$  at Dome C was larger than that at Dome Fuji in MIROC5-iso  
 209 and the ice core records, whereas the opposite is modeled in ECHAM6-wiso. Despite the need to  
 210 consider such inter-model discrepancies, our results are reasonable for discussing Antarctic  $\delta^{18}\text{O}_p$   
 211 in the LGM.

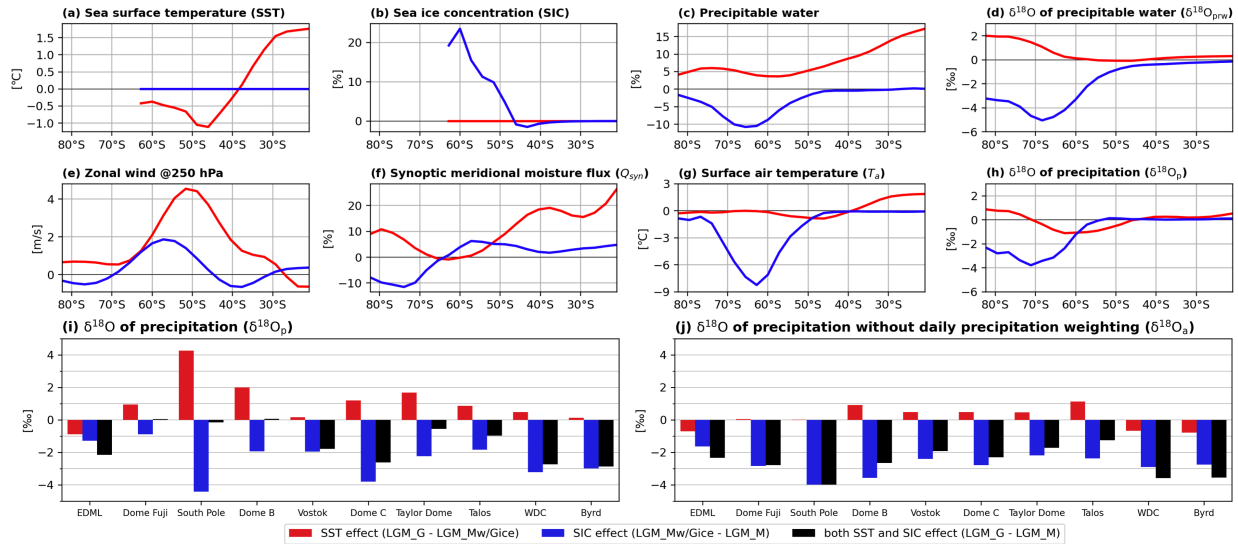
212 In contrast to  $\Delta\delta^{18}\text{O}_p$ , simulated  $\Delta T_a$  in LGM\_G and LGM\_M varied slightly (Figure  
 213 S4b). Our simulation underestimated the cooling reconstructed from ice cores of EDML, Dome  
 214 Fuji, Dome B, Vostok, and Dome C and overestimated that from Taylor Dome, Talos, WDC,  
 215 and Byrd.

216

217 3.2 Role of the atmospheric circulation in determining  $\Delta\delta^{18}\text{O}_p$  in interior Antarctica  
218 during the last glacial maximum

219 In this section, we discuss the processes contributing to  $\delta^{18}\text{O}_p$  values in Antarctica in  
 220 relation to the mid-latitude atmospheric circulations. Across PI and LGM experiments, the  
 221 southward moisture transports were mostly maintained in  $Q_{\text{syn}}$ , followed by  $Q_{\text{LF}}$ , with minimal  
 222 contribution from  $Q_m$  (Figure S6), consistent with the reanalysis data (Newman et al., 2012).  
 223 Such results highlight the importance of understanding changes in  $Q_{\text{syn}}$  across the experiments  
 224 to discuss the processes contributing to Antarctic  $\delta^{18}\text{O}_p$ . To this end, we decoupled the individual

225 effects of SST and SIC on the southern mid-high latitudes climate including  $Q_{syn}$  and Antarctic  
 226  $\delta^{18}O_p$  by comparing LGM\_Mw/Gice sensitivity experiments with LGM\_G and LGM\_M.  
 227



228  
 229 **Figure 1** Sea surface temperature (SST) and sea ice (SIC) substitution impact the southern hemisphere climate.  
 230 The red and blue curves and bars represent changes due to SST (from LGM\_Mw/Gice to LGM\_G) and SIC  
 231 (from LGM\_M to LGM\_Mw/Gice). Zonal mean changes in (a) SST, (b) SIC, (c) precipitable water, (d)  $\delta^{18}O$   
 232 of precipitable water ( $\delta^{18}O_{prw}$ ), (e) zonal wind at 250hPa, (f) synoptic meridional moisture flux ( $Q_{syn}$ ), (g)  
 233 surface air temperature ( $T_a$ ), (h)  $\delta^{18}O$  of precipitation ( $\delta^{18}O_p$ ). Changes in (i)  $\delta^{18}O_p$  and (j)  $\delta^{18}O_p$  without daily  
 234 precipitation weighting ( $\delta^{18}O_a$ , see Text S2) at 10 Antarctic sites. For (b), (c), and (f), changes are shown as  
 235 ratios, while for the remaining panels, they are presented as anomalies. For (e) and (f), the eastward and  
 236 southward directions are indicated as positive, respectively. For (i) and (j), changes due to the combination of  
 237 both SST and SIC (from LGM\_M to LGM\_G) are also shown. Each site location is presented in Figure 2a.  
 238

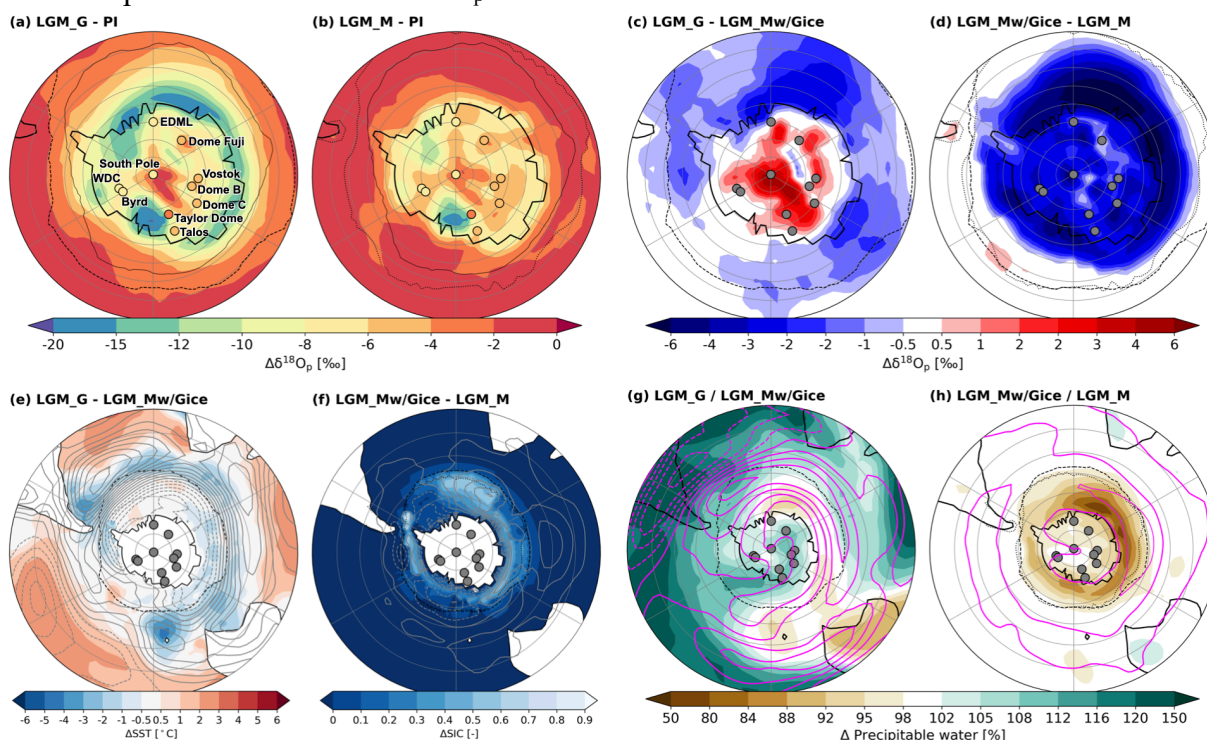
### 239 3.2.1 SST substitution impacts (LGM\_G minus LGM\_Mw/Gice)

240 We investigated the effects of SST substitution from LGM\_Mw/Gice to LGM\_G in  
 241 relation to the mid-latitude atmospheric circulation. The SST substitution warmed (cooled) SST  
 242 at the north (south) of  $\sim 40^\circ S$  (Figures 1a), increased (decreased) evaporation and sensible heat  
 243 fluxes (Figures S7b–c). The increase in the Eady growth rate along the SST front (Figure S8),  
 244 suggesting a stronger baroclinic instability, illustrates the role of the steepened meridional SST  
 245 gradient (Figure S7a). These circulation changes enhanced the southward moisture fluxes,  
 246 resulting from elevations in both humidity and southward winds (Figures S7f, 1c, and S7e).

247 The elevations in southward moisture fluxes described above predominantly occurred on  
 248 the synoptic scale. The strengthened  $Q_{syn}$  by 5–10% increased the precipitable water by  $\sim 5\%$   
 249 south of  $\sim 70^\circ S$  (Figures 1f and 1c), resulting in an increase in the  $\delta^{18}O$  of precipitable water  
 250 ( $\delta^{18}O_{prw}$ ) and  $\delta^{18}O_p$  by  $\sim 2\text{‰}$  and  $\sim 1\text{‰}$ , respectively, south of  $\sim 70^\circ S$  (Figures 1d and 1h). The  
 251 zonal mean  $Q_{LF}$  changed slightly south of  $\sim 70^\circ S$  (Figure S7h). However, low-frequency  
 252 variations in atmospheric circulation were not the primary factor but could indirectly influence  
 253 the moisture fluxes through the synoptic circulations (Kino et al., 2021). The zonal mean  $Q_m$

254 increased north of  $\sim 60^\circ\text{S}$ , but not south of  $\sim 60^\circ\text{S}$  (Figure S7g). The strengthened westerly jet  
 255 (Figure 1e) was associated with the steepened meridional SST (Ogawa et al., 2016).

256 The spatially heterogeneous changes in  $\Delta\delta^{18}\text{O}_p$  values in Antarctica (Figure 2c) can be  
 257 partly attributed to the regional dominant atmospheric patterns (Kino et al., 2021; Marshall et al.,  
 258 2017; Marshall & Thompson, 2016). Figure 2g shows an increase in the moisture inflow  
 259 extended from the Ross Sea and West Antarctica, where the changes in sea level pressures and  
 260 zonal winds were moderate (contours in Figures 2e and 2g), to East Antarctica. It suggests the  
 261 importance of the southerly advection (Dittman et al., 2016; Schlosser et al., 2017) for moisture  
 262 inflow. We analyzed the climatological  $\delta^{18}\text{O}_p$  without daily precipitation weighting (hereafter  
 263 referred to as  $\delta^{18}\text{O}_a$ , see Text S2) to evaluate the impacts of EPEs (Figure 1j). The small absolute  
 264 values of  $\Delta\delta^{18}\text{O}_a$  indicate that the effects of SST substitution were mostly related to EPEs.  
 265 Moreover, the spatial heterogeneity of  $\Delta\delta^{18}\text{O}_p$  minus  $\Delta\delta^{18}\text{O}_a$  was pronounced (Figure S9a),  
 266 indicating the contribution of the EPEs to  $\Delta\delta^{18}\text{O}_p$  was uneven among sites. The southerly  
 267 advection (Dittman et al., 2016; Schlosser et al., 2017) and various blocking patterns related to  
 268 EPEs (Wang et al., 2023), along with variations in their occurrence frequency, would explain the  
 269 relationship between EPEs and  $\Delta\delta^{18}\text{O}_p$ .



270  
 271 **Figure 2** Climatological anomalies. **(a)**  $\delta^{18}\text{O}$  of precipitation ( $\delta^{18}\text{O}_p$ ) changes from Pre-Industrial (PI) to  
 272 LGM\_G in  $50\text{--}90^\circ\text{S}$ . **(b)** As in **(a)**, but for PI to LGM\_M. **(c)**–**(d)** Changes due to sea surface temperature  
 273 (SST) and sea ice concentration (SIC) substitutions: **(c)** from LGM\_Mw/Gice to LGM\_G; **(d)** from  
 274 LGM\_Mw/Gice to LGM\_M. **(e)**–**(f)** As in **(c)**–**(d)**, but for SST and SIC, respectively, (shades) and sea level  
 275 pressure (SLP; gray contours in every 0.5 hPa) in  $20\text{--}90^\circ\text{S}$ . **(g)**–**(h)** As in **(c)**–**(d)**, but for precipitable water  
 276 (shades) and zonal winds at 250 hPa (magenta contours in every 2 m/s) in  $20\text{--}90^\circ\text{S}$ . For precipitable water in  
 277 panels **(g)**–**(h)**, changes are presented as ratios, while for the remaining variables and panels, they are presented  
 278 as anomalies. Positive anomalies for SLP and zonal winds are depicted with solid gray and magenta contours,  
 279 respectively, while negative anomalies are dashed. Each panel denotes 15% SIC in PI, GLOMAP, and MIROC  
 280 (thin solid, thick dashed, and thick dotted black contours, respectively). Each panel also denotes 10 Antarctic

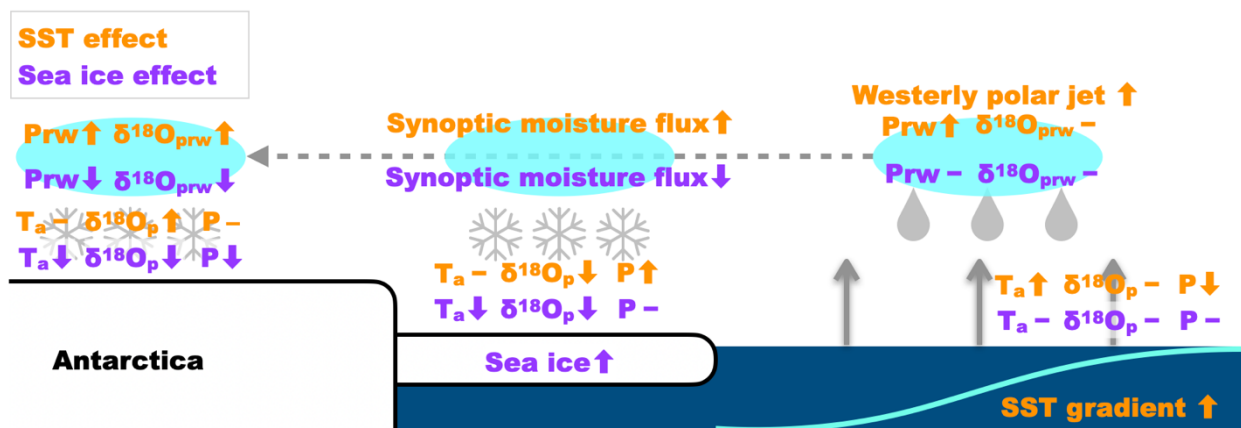
281 ice core sites with circles; for (a)–(b), these are overlaid with  $\Delta\delta^{18}\text{O}_{\text{ice}}$ . Refer to Section 2.2 for specifics on the  
 282 sites.

283 3.2.2. SIC substitution impacts (LGM\_Mw/Gice minus LGM\_M)

284 We investigated the effects of SIC substitution from LGM\_M to LGM\_Mw/Gice,  
 285 specifically SIC expansion in SH (Figure 1b), with respect to atmospheric circulation. In contrast  
 286 to the SST substitution case,  $Q_{\text{syn}}$  decreased by  $\sim 10\%$  and was partly compensated by  $Q_m$  south  
 287 of  $\sim 70^\circ\text{S}$  (Figures 1f and S7g). The precipitable water decreased by  $\sim 5\%$  south of  $\sim 70^\circ\text{S}$  and  
 288  $\sim 10\%$  in  $60\text{--}70^\circ\text{S}$ , affected by strong cooling over SI (Figures 1c and 1g). The  $T_a$  reduction  
 289 promoted isotopic fractionation during the transport from the open ocean to Antarctica.  
 290 Combined with the extended transport pathway (Kohfeld et al., 2013; Sime et al., 2013, 2016),  
 291  $\delta^{18}\text{O}_{\text{prw}}$  decreased extensively around Antarctica, resulting in  $\delta^{18}\text{O}_p$  decreases by  $\sim 3\text{‰}$  south of  
 292  $\sim 70^\circ\text{S}$  (Figures 1d and 1h).

293 The reduction was strong in  $\delta^{18}\text{O}_a$ , too (Figure 1j), suggesting that the SIC substitution  
 294 changed the mean isotopic environment around Antarctica and that EPEs were not the main  
 295 controlling factor on  $\delta^{18}\text{O}$  in precipitation. Nevertheless, the effects of SIC substitution on the  
 296 EPEs were evidenced by the more pronounced variations in  $\Delta\delta^{18}\text{O}_p$  than  $\Delta\delta^{18}\text{O}_a$  among the sites  
 297 (Figures 1i–j). The mean circulation changes due to the SIC substitution can explain such  
 298 spatially uneven influences of EPEs. SIC anomaly between LGM\_Mw/Gice and LGM\_M was  
 299 zonally non-uniform, particularly evident in the region in  $\sim 0\text{--}120^\circ\text{E}$  (Figure 2f). This localized  
 300 SIC expansion eased the stagnation of Rossby waves and reduced precipitable water (Figure 2h).  
 301 Such blocking can influence oceanic inflows, thus affecting  $\Delta\delta^{18}\text{O}_p$  minus  $\Delta\delta^{18}\text{O}_a$  around Dome  
 302 Fuji and Dome B (Figure S9).  
 303

304 **4. Influence of sea surface conditions on southward moisture transport and  $\delta^{18}\text{O}_p$  in inner**  
 305 **Antarctica: discussion and perspectives**



306 **Figure 3** Schematic view of the processes ruling the  $\Delta\delta^{18}\text{O}_p$  in inland Antarctica during LGM. The orange and  
 307 purple colors represent the key processes associated with the substitution of SST (LGM\_G minus  
 308 LGM\_Mw/Gice) and SIC (LGM\_Mw/Gice minus LGM\_M), respectively. The upward and downward arrows  
 309 represent the increases and decreases of the values of the variables, respectively.  
 310  
 311

312 Our results revealed that the sea surface conditions influence southward moisture  
 313 transport and  $\delta^{18}\text{O}_p$  in inland Antarctica through synoptic circulations. Figure 3 illustrates the  
 314 main findings of our study. To estimate these quantitative contributions, spatially heterogeneous

315  $\Delta \delta^{18}\text{O}$  could be crucial. The impacts of the SST and SIC substitutions differed among sites,  
316 particularly with respect to EPEs. Appropriate sea surface conditions, atmospheric circulations,  
317 and Antarctic precipitation intensities are essential for adequately representing  $\delta^{18}\text{O}_{\text{ice}}$  in iso-  
318 GCMs. Our three LGM experiments indicate that the synoptic circulations in the southern mid-  
319 latitudes, overlooked in studies utilizing the classical one-dimensional isotope model approach,  
320 are crucial in understanding  $\delta^{18}\text{O}_{\text{p}}$  in inland Antarctica during the LGM. The spatial relationship  
321 of  $\Delta \delta^{18}\text{O}_{\text{ice}}$  across Antarctic ice core sites could be a reliable indicator of these atmospheric  
322 circulations. Our study further suggests that investigating Antarctic ice cores with iso-GCMs can  
323 aid in more precisely constraining the behavior of LGM southern westerlies, which affect the SO  
324 circulation that traps atmospheric  $\text{CO}_2$  in the deep ocean (Toggweiler et al., 2006).

325 Certain biases in MIROC5-iso and methodological limitations underscore the need for  
326 enhanced modeling to constrain LGM climate. MIROC5-iso overestimated summer precipitation  
327 intensity at Dome Fuji in the modern climate, possibly because of its low spatial resolution (Kino  
328 et al., 2021). Such bias would affect  $\Delta \delta^{18}\text{O}_{\text{p}}$  and its relationship with  $\Delta T_a$  and partly explain the  
329 spatial inconsistency between MIROC5-iso and ECHAM6-wiso in T63 (Cauquoin et al., 2023).  
330 Detailed comparisons among iso-GCMs are needed for more optimized constraints of the LGM  
331 climate. The westerly jets of the MIROC5 are biased equatorward in the modern climate  
332 (Watanabe et al., 2010). This bias may be associated with the features of westerlies and synoptic  
333 circulations in the LGM. Internal variability should also be discussed. The climatological  $\delta^{18}\text{O}_{\text{p}}$   
334 was determined by a combination of multiple moisture transport patterns, including blocking  
335 (Dittmann et al., 2016; Schlosser et al., 2017; Wang et al., 2023); 30-year analyses may be  
336 insufficient to evaluate the frequency of each pattern.

337 Further experiments forced by idealized SST and SIC (e.g., zonally uniform) will be  
338 performed to isolate and examine more precisely the impacts of SST gradients on atmospheric  
339 dynamics, leading to a better understanding of the mechanisms linking sea surface conditions to  
340 Antarctic  $\delta^{18}\text{O}_{\text{p}}$ . Evaluating d-excess profiles would also aid in establishing the connection  
341 between SST of the moisture source regions reconstructed from ice cores (Uemura et al., 2018)  
342 and the role of SST and SIC identified in this study. Further investigation is required to  
343 determine the effects of changes in ice-sheet elevation (Werner et al., 2018), precipitation  
344 seasonality (Erb et al., 2018), and the inversion layer depths (Buizert et al., 2021) on  $\delta^{18}\text{O}_{\text{p}}$  in  
345 inland Antarctica. The global reproducibility of LGM climates is also important for more  
346 optimized Antarctic temperature estimations, as  $\delta^{18}\text{O}_{\text{p}}$  in inland Antarctica is associated with the  
347 broader southern hemisphere. The two sets of LGM sea surface conditions used in this study  
348 were not the end members of PMIP models (Kageyama, Harrison, et al., 2021). Multiple LGM  
349 simulations would be required to constrain the LGM Antarctic temperatures.

350

## 351 **Acknowledgments**

352 • The first author was supported by the Japan Society for the Promotion of Science (JSPS) via  
353 a Grant-in-Aid for JSPS Fellows.

354 • This work was supported by the Japan Society for the Promotion of Science (JSPS) via

355 Grants-in-Aid 17K14397, 19J14488, 21H05002, 22K14095, 22K21323, and JSPs-LEAD

356 with DFG via 416767181, and the Integrated Research Program for Advancing Climate  
357 Models (TOUGOU; JPMXD0717935457), ArCS II (JP-MXD1420318865), DIAS  
358 (JPMXD0716808979), and the advanced studies of climate change projection (SENTAN;  
359 JPMXD0722680395) from the Ministry of Education, Culture, Sports, Science and  
360 Technology (MEXT), Japan, and the Environment Research and Technology Development  
361 Fund S-20 (Grant Number JPMEERF21S12020) from the Environmental Restoration and  
362 Conservation Agency of Japan.

363 • We also thank Masakazu Yoshimori, Yukari Takayabu, Masahiro Watanabe, Hisashi  
364 Nakamura, Yukio Masumoto, Masahide Kimoto, Fumiaki Ogawa, and Satoru Okajima for  
365 their constructive comments.

366

### 367 **Open Research**

- 368 • Ice core data used for Figures S2 and S3 are available at [https://www.ncdc.noaa.gov/data-](https://www.ncdc.noaa.gov/data-access/paleoclimatology-data)  
369 [access/paleoclimatology-data](https://www.ncdc.noaa.gov/data-access/paleoclimatology-data) and are reported in Cauquoin et al. (2019). Ice core data used  
370 for Figures 1i and 2a–b, except for the South Pole, are available in Table 1 of Werner et al.  
371 (2018). Data for the South Pole is available at <https://doi.org/10.15784/601239> (E. J. Steig et  
372 al., 2020). The SISAL speleothem dataset is available at <https://doi.org/10.17864/1947.256>  
373 (Comas-Bru, Atsawawaranunt, et al., 2020). The GLOMAP is available at  
374 <https://doi.pangaea.de/10.1594/PANGAEA.923262> (Paul et al., 2020). The SST and SIC  
375 outputs from MIROC4m-AOGCM are available from the authors of Sherriff-Tadano et al.  
376 (2023).
- 377 • The code of the isotopic version MIROC5-iso is available upon request on the IIS's GitLab  
378 repository (<http://isotope.iis.u-tokyo.ac.jp:8000/gitlab/miroc-iso/miroc5-iso>, Okazaki and  
379 Yoshimura, 2019).

- 380 • The source codes and data used in this study are available at  
381 <https://github.com/kanonundgigue/kino2024grl> and  
382 <https://zenodo.org/doi/10.5281/zenodo.7582875> (Kino et al., 2024).

383

#### 384 **References**

- 385 Augustin, L., Barbante, C., Barnes, P. R. F., Barnola, J. M., Bigler, M., Castellano, E., et al.  
386 (2004). Eight glacial cycles from an Antarctic ice core. *Nature*, *429*(6992), 623–628.  
387 <https://doi.org/10.1038/nature02599>
- 388 Augustin, L., Barbante, C., Barnes, P. R. F., Barnola, J. M., Bigler, M., Castellano, E., et al.  
389 (2004). Eight glacial cycles from an Antarctic ice core. *Nature*, *429*(6992), 623–628.  
390 <https://doi.org/10.1038/nature02599>
- 391 Ayako Abe-Ouchi, F. Saito, K. Kawamura, M. Raymo, J. Okuno, K. Takahashi, and H.  
392 Blatter: Insolation-driven 100,000-year glacial cycles and hysteresis of ice-sheet volume,  
393 *Nature*, *500*, 190–193, 2013, doi:10.1038/nature12374
- 394 Briggs, R. D., Pollard, D., & Tarasov, L. (2014). A data-constrained large ensemble analysis of  
395 Antarctic evolution since the Eemian. *Quaternary Science Reviews*, *103*, 91–115.  
396 <https://doi.org/10.1016/j.quascirev.2014.09.003>
- 397 Buizert, C., Fudge, T. J., Roberts, W. H. G., Steig, E. J., Sherriff-Tadano, S., Ritz, C., et al. (2021).  
398 Antarctic surface temperature and elevation during the Last Glacial Maximum. *Science*,  
399 *372*(6546), 1097–1101. <https://doi.org/10.1126/science.abd2897>
- 400 Cauquoin, A., Abe-Ouchi, A., Obase, T., Chan, W.-L., Paul, A., & Werner, M. (2023). Effects of  
401 Last Glacial Maximum (LGM) sea surface temperature and sea ice extent on the isotope–  
402 temperature slope at polar ice core sites. *Climate of the Past*, *19*(6), 1275–1294.  
403 <https://doi.org/10.5194/cp-19-1275-2023>

- 404 Cauquoin, A., Abe-Ouchi, A., Obase, T., Chan, W.-L., Paul, A., & Werner, M. (2023). Effects of  
405 Last Glacial Maximum (LGM) sea surface temperature and sea ice extent on the isotope–  
406 temperature slope at polar ice core sites. *Climate of the Past*, *19*(6), 1275–1294.  
407 <https://doi.org/10.5194/cp-19-1275-2023>
- 408 Cauquoin, A., Risi, C., & Vignon, É. (2019). Importance of the advection scheme for the  
409 simulation of water isotopes over Antarctica by atmospheric general circulation models: A  
410 case study for present-day and Last Glacial Maximum with LMDZ-iso. *Earth and  
411 Planetary Science Letters*, *524*, 115731. <https://doi.org/10.1016/j.epsl.2019.115731>
- 412 Cauquoin, A., Werner, M., & Lohmann, G. (2019). Water isotopes – climate relationships for the  
413 mid-Holocene and preindustrial period simulated with an isotope-enabled version of MPI-  
414 ESM. *Climate of the Past*, *15*(6), 1913–1937. <https://doi.org/10.5194/cp-15-1913-2019>
- 415 Comas-Bru, L., Atsawawaranunt, K., Harrison, S., & SISAL working group members. (2020).  
416 SISAL (Speleothem Isotopes Synthesis and AnaLysis Working Group) database version  
417 2.0 [Data set]. University of Reading. <https://doi.org/10.17864/1947.256>
- 418 Comas-Bru, L., Harrison, S. P., Werner, M., Rehfeld, K., Scropton, N., Veiga-Pires, C., & SISAL  
419 working group members. (2019). Evaluating model outputs using integrated global  
420 speleothem records of climate change since the last glacial. *Climate of the Past*, *15*(4),  
421 1557–1579. <https://doi.org/10.5194/cp-15-1557-2019>
- 422 Comas-Bru, L., Rehfeld, K., Roesch, C., Amirnezhad-Mozhdehi, S., Harrison, S. P.,  
423 Atsawawaranunt, K., et al. (2020, March 13). SISALv2: A comprehensive speleothem  
424 isotope database with multiple age-depth models. *Earth System Science Data Discussions*.  
425 <https://doi.org/10.5194/essd-2020-39>

- 426 Dahe, Q., Petit, J. R., Jouzel, J., & Stievenard, M. (1994). Distribution of stable isotopes in surface  
427 snow along the route of the 1990 International Trans-Antarctica Expedition. *Journal of*  
428 *Glaciology*, 40(134), 107–118. <https://doi.org/10.3189/S0022143000003865>
- 429 Dahe, Q., Petit, J. R., Jouzel, J., & Stievenard, M. (1994). Distribution of stable isotopes in surface  
430 snow along the route of the 1990 International Trans-Antarctica Expedition. *Journal of*  
431 *Glaciology*, 40(134), 107–118. <https://doi.org/10.3189/S0022143000003865>
- 432 Dansgaard, W. (1964). Stable isotopes in precipitation. *Tell'Us*, 16(4), 436–468.  
433 <https://doi.org/10.3402/tellusa.v16i4.8993>
- 434 Dittmann, A., Schlosser, E., Masson-Delmotte, V., Powers, J. G., Manning, K. W., Werner, M., &  
435 Fujita, K. (2016). Precipitation regime and stable isotopes at Dome Fuji, East Antarctica.  
436 *Atmospheric Chemistry and Physics*, 16(11), 6883–6900. [https://doi.org/10.5194/acp-16-](https://doi.org/10.5194/acp-16-6883-2016)  
437 [6883-2016](https://doi.org/10.5194/acp-16-6883-2016)
- 438 Erb, M. P., Jackson, C. S., Broccoli, A. J., Lea, D. W., Valdes, P. J., Crucifix, M., & DiNezio, P.  
439 N. (2018). Model evidence for a seasonal bias in Antarctic ice cores. *Nature*  
440 *Communications*, 9(1), 1361. <https://doi.org/10.1038/s41467-018-03800-0>
- 441 Eyring, V., Bony, S., Meehl, G. A., Senior, C. A., Stevens, B., Stouffer, R. J., & Taylor, K. E.  
442 (2016). Overview of the Coupled Model Intercomparison Project Phase 6 (CMIP6)  
443 experimental design and organization. *Geoscientific Model Development*, 9(5), 1937–1958.  
444 <https://doi.org/10.5194/gmd-9-1937-2016>
- 445 Fujita, K., & Abe, O. (2006). Stable isotopes in daily precipitation at Dome Fuji, East Antarctica.  
446 *Geophysical Research Letters*, 33(18). <https://doi.org/10.1029/2006GL026936>

- 447 Hirasawa, N., Nakamura, H., & Yamanouchi, T. (2000). Abrupt changes in meteorological  
448 conditions observed at an inland Antarctic Station in association with wintertime blocking.  
449 *Geophysical Research Letters*, 27(13), 1911–1914. <https://doi.org/10.1029/1999gl011039>
- 450 Hirasawa, N., Nakamura, H., Motoyama, H., Hayashi, M., & Yamanouchi, T. (2013). The role of  
451 synoptic-scale features and advection in prolonged warming and generation of different  
452 forms of precipitation at Dome Fuji station, Antarctica, following a prominent blocking  
453 event. *Journal of Geophysical Research*, 118(13), 6916–6928.  
454 <https://doi.org/10.1002/jgrd.50532>
- 455 Ivanovic, Gregoire, Kageyama, Roche, Valdes, Burke, et al. (2016). Transient climate simulations  
456 of the deglaciation 21--9 thousand years before present (version 1) -- PMIP4 Core  
457 experiment design and boundary conditions. *Geoscientific Model Development*, 9(7),  
458 2563–2587.
- 459 Kageyama, M., Abe-Ouchi, A., Obase, T., Ramstein, G., & Valdes, P. J. (2021). Modeling the  
460 climate of the last glacial maximum from PMIP1 to PMIP4. In P. B. A. K. J. M. Paul J.  
461 Valdes (Ed.) (Vol. 29, pp. 80–81). Past Global Changes (PAGES).  
462 <https://doi.org/10.22498/pages.29.2.80>
- 463 Kageyama, M., Albani, S., Braconnot, P., Harrison, S. P., Hopcroft, P. O., Ivanovic, R. F., et al.  
464 (2017). The PMIP4 contribution to CMIP6 -- Part 4: Scientific objectives and experimental  
465 design of the PMIP4-CMIP6 Last Glacial Maximum experiments and PMIP4 sensitivity  
466 experiments. *Geoscientific Model Development*, 10(11), 4035–4055. Retrieved from  
467 <https://gmd.copernicus.org/articles/10/4035/2017/>
- 468 Kageyama, M., Harrison, S. P., Kapsch, M.-L., Lofverstrom, M., Lora, J. M., Mikolajewicz, U., et  
469 al. (2021). The PMIP4 Last Glacial Maximum experiments: preliminary results and

- 470 comparison with the PMIP3 simulations. *Climate of the Past*, 17(3), 1065–1089.  
471 <https://doi.org/10.5194/cp-17-1065-2021>
- 472 Kawamura, K., Abe-Ouchi, A., Motoyama, H., Ageta, Y., Aoki, S., Azuma, N., et al. (2017). State  
473 dependence of climatic instability over the past 720,000 years from Antarctic ice cores and  
474 climate modeling. *Science Advances*, 3(2), e1600446.  
475 <https://doi.org/10.1126/sciadv.1600446>
- 476 Kawamura, K., Parrenin, F., Lisiecki, L., Uemura, R., Vimeux, F., Severinghaus, J. P., et al.  
477 (2007). Northern Hemisphere forcing of climatic cycles in Antarctica over the past 360,000  
478 years. *Nature*, 448(7156), 912–916. <https://doi.org/10.1038/nature06015>
- 479 Kino, K., Okazaki, A., Cauquoin, A., & Yoshimura, K. (2021). Contribution of the southern  
480 annular mode to variations in water isotopes of daily precipitation at dome Fuji, east  
481 Antarctica. *Journal of Geophysical Research*, 126(23), e2021JD035397.  
482 <https://doi.org/10.1029/2021jd035397>
- 483 Kino, K., Okazaki, A., Cauquoin, A., & Yoshimura, K. (2021). Contribution of the southern  
484 annular mode to variations in water isotopes of daily precipitation at dome Fuji, east  
485 Antarctica. *Journal of Geophysical Research*, 126(23).  
486 <https://doi.org/10.1029/2021jd035397>
- 487 Kohfeld, K. E., Graham, R. M., de Boer, A. M., Sime, L., Wolff, E. W., Le Quéré, C., & Bopp, L.  
488 (2013). Southern Hemisphere westerly wind changes during the Last Glacial Maximum:  
489 paleo-data synthesis. *Quaternary Science Reviews*, 68, 76–95.  
490 <https://doi.org/10.1016/j.quascirev.2013.01.017>

- 491 Krinner, G., & Werner, M. (2003). Impact of precipitation seasonality changes on isotopic signals  
492 in polar ice cores: a multi-model analysis. *Earth and Planetary Science Letters*, 216(4),  
493 525–538. [https://doi.org/10.1016/S0012-821X\(03\)00550-8](https://doi.org/10.1016/S0012-821X(03)00550-8)
- 494 Landais, A., Dreyfus, G., Capron, E., Jouzel, J., Masson-Delmotte, V., Roche, D. M., et al. (2013).  
495 Two-phase change in CO<sub>2</sub>, Antarctic temperature and global climate during Termination  
496 II. *Nature Geoscience*, 6(12), 1062–1065. <https://doi.org/10.1038/ngeo1985>
- 497 Lee, J.-E., Fung, I., DePaolo, D. J., & Otto-Bliesner, B. (2008). Water isotopes during the Last  
498 Glacial Maximum: New general circulation model calculations. *Journal of Geophysical*  
499 *Research*, 113(D19), 1341. <https://doi.org/10.1029/2008JD009859>
- 500 Lev Tarasov and W. Richard Peltier Greenland glacial history and local geodynamic  
501 consequences, *Geophysical Journal International*, 150, July 2002, Pages 198-  
502 229, doi:10.1046/j.1365-246X.2002.01702.x
- 503 Tarasov, L., Hughes, A., Gyllencreutz, R., Lohne, O.S., Mangerud, J., & Svendsen, J.I. The global  
504 GLAC-1c deglaciation chronology, meltwater pulse 1-a, and a question of missing ice, IGS  
505 Symposium on Contribution of Glaciers and Ice-sheets to Sea-Level Change, 2014
- 506 Lorius, C., & Merlivat, L. (1977). Distribution of mean surface stable isotope values in East  
507 Antarctica, Isotopes and Impurities in Snow and Ice. *International Association of*  
508 *Hydrological Sciences, Publication*, 118, 127–137.
- 509 Lorius, C., Merlivat, L., Jouzel, J., & Pourchet, M. (1979). A 30,000-yr isotope climatic record  
510 from Antarctic ice. *Nature*, 280(5724), 644–648. <https://doi.org/10.1038/280644a0>
- 511 Marshall, G. J., & Thompson, D. W. J. (2016). The signatures of large-scale patterns of  
512 atmospheric variability in Antarctic surface temperatures. *Journal of Geophysical*  
513 *Research*, 121(7), 3276–3289. <https://doi.org/10.1002/2015jd024665>

- 514 Marshall, G. J., Thompson, D. W. J., & van den Broeke, M. R. (2017). The Signature of Southern  
515 Hemisphere Atmospheric Circulation Patterns in Antarctic Precipitation. *Geophysical*  
516 *Research Letters*, 44(22), 11580–11589. <https://doi.org/10.1002/2017GL075998>
- 517 Motoyama, H. (2005). Seasonal variations in oxygen isotope ratios of daily collected precipitation  
518 and wind drift samples and in the final snow cover at Dome Fuji Station, Antarctica.  
519 *Journal of Geophysical Research*, 110(D11). <https://doi.org/10.1029/2004JD004953>
- 520 Nakamura, H., Sampe, T., Goto, A., Ohfuchi, W., & Xie, S.-P. (2008). On the importance of  
521 midlatitude oceanic frontal zones for the mean state and dominant variability in the  
522 tropospheric circulation. *Geophysical Research Letters*, 35(15).  
523 <https://doi.org/10.1029/2008GL034010>
- 524 Newman, M., Kiladis, G. N., Weickmann, K. M., Martin Ralph, F., & Sardeshmukh, P. D. (2012).  
525 Relative Contributions of Synoptic and Low-Frequency Eddies to Time-Mean Atmospheric  
526 Moisture Transport, Including the Role of Atmospheric Rivers. *Journal of Climate*, 25(21),  
527 7341–7361. <https://doi.org/10.1175/JCLI-D-11-00665.1>
- 528 Noone, D., & Simmonds, I. (2002). Annular variations in moisture transport mechanisms and the  
529 abundance of  $\delta^{18}\text{O}$  in Antarctic snow. *Journal of Geophysical Research*, 107(D24), 4742.  
530 <https://doi.org/10.1029/2002JD002262>
- 531 Ogawa, F., Nakamura, H., Nishii, K., Miyasaka, T., & Kuwano-Yoshida, A. (2016). Importance of  
532 Midlatitude Oceanic Frontal Zones for the Annular Mode Variability: Interbasin  
533 Differences in the Southern Annular Mode Signature. *Journal of Climate*, 29(17), 6179–  
534 6199. <https://doi.org/10.1175/JCLI-D-15-0885.1>

- 535 Okazaki, A., & Yoshimura, K. (2017). Development and evaluation of a system of proxy data  
536 assimilation for paleoclimate reconstruction. *Climate of the Past*, 13(4), 379–393.  
537 <https://doi.org/10.5194/cp-13-379-2017>
- 538 Okazaki, A., & Yoshimura, K. (2019). Global evaluation of proxy system models for stable water  
539 isotopes with realistic atmospheric forcing. *Journal of Geophysical Research*, 124(16),  
540 8972–8993. <https://doi.org/10.1029/2018jd029463>
- 541 Paul, A., Mulitza, S., Stein, R., & Werner, M. (2020). Glacial Ocean Map (GLOMAP) [Data set].  
542 PANGAEA. <https://doi.org/10.1594/PANGAEA.923262>
- 543 Paul, A., Mulitza, S., Stein, R., & Werner, M. (2021). A global climatology of the ocean surface  
544 during the Last Glacial Maximum mapped on a regular grid (GLOMAP). *Climate of the*  
545 *Past*, 17(2), 805–824. <https://doi.org/10.5194/cp-17-805-2021>
- 546 Risi, C., Bony, S., Vimeux, F., & Jouzel, J. (2010). Water-stable isotopes in the LMDZ4 general  
547 circulation model: Model evaluation for present-day and past climates and applications to  
548 climatic interpretations of tropical isotopic records. *Journal of Geophysical Research*,  
549 115(D12), 108. <https://doi.org/10.1029/2009jd013255>
- 550 Satow, K., Watanabe, O., Shoji, H., & Motoyama, H. (1999). The relationship among  
551 accumulation rate, stable isotope ratio and surface temperature on the plateau of east  
552 Dronning Maud Land, Antarctica. *Polar Meteorology and Glaciology*, 13, 43–52.  
553 <https://doi.org/10.15094/00002888>
- 554 Schlosser, E., Dittmann, A., Stenni, B., Powers, J. G., Manning, K. W., Masson-Delmotte, V., et  
555 al. (2017). The influence of the synoptic regime on stable water isotopes in precipitation at  
556 Dome C, East Antarctica. *The Cryosphere*, 11(5), 2345–2361. [https://doi.org/10.5194/tc-](https://doi.org/10.5194/tc-11-2345-2017)  
557 [11-2345-2017](https://doi.org/10.5194/tc-11-2345-2017)

- 558 Schlosser, E., Manning, K. W., Powers, J. G., Duda, M. G., Birnbaum, G., & Fujita, K. (2010).  
559 Characteristics of high-precipitation events in Dronning Maud Land, Antarctica. *Journal of*  
560 *Geophysical Research*, 115(D14), 3518. <https://doi.org/10.1029/2009JD013410>
- 561 Servettaz, A. P. M., Orsi, A. J., Curran, M. A. J., Moy, A. D., Landais, A., Agosta, C., et al.  
562 (2020). Snowfall and water stable isotope variability in east Antarctica controlled by warm  
563 synoptic events. *Journal of Geophysical Research*, 125(17).  
564 <https://doi.org/10.1029/2020jd032863>
- 565 Sherriff-Tadano, S., & Klockmann, M. (2021). PMIP contributions to understanding the deep  
566 ocean circulation of the Last Glacial Maximum. *Past Global Change Magazine*, 29(2), 84–  
567 85. <https://doi.org/10.22498/pages.29.2.84>
- 568 Sherriff-Tadano, S., Abe-Ouchi, A., Yoshimori, M., Hotta, H., Kikuchi, M., Ohgaito, R., et al.  
569 (2023). Southern Ocean surface temperatures and cloud biases in climate models connected  
570 to the representation of glacial deep ocean circulation. *Journal of Climate*.
- 571 Sime, L., & Wolff, E. W. (2011, November 9). Antarctic accumulation seasonality. *Nature*.  
572 <https://doi.org/10.1038/nature10613>
- 573 Sime, L., Hodgson, D., Bracegirdle, T. J., Allen, C., Perren, B., Roberts, S., & de Boer, A. M.  
574 (2016). Sea ice led to poleward-shifted winds at the Last Glacial Maximum: the influence  
575 of state dependency on CMIP5 and PMIP3 models. *Climate of the Past*, 12(12), 2241–  
576 2253. <https://doi.org/10.5194/cp-12-2241-2016>
- 577 Sime, L., Kohfeld, K. E., Le Quéré, C., Wolff, E. W., de Boer, A. M., Graham, R. M., & Bopp, L.  
578 (2013). Southern Hemisphere westerly wind changes during the Last Glacial Maximum:  
579 model-data comparison. *Quaternary Science Reviews*, 64, 104–120.  
580 <https://doi.org/10.1016/j.quascirev.2012.12.008>

- 581 Steig, E. J., Jones, T. R., Kahle, E., Morris, V., Schauer, A., Vaughn, B., & White, J. (2020). South  
582 Pole high resolution ice core water stable isotope record for dD, d18O [Data set]. South  
583 Pole high resolution ice core water stable isotope record for dD, d18O. Antarctic Program  
584 (USAP) Data Center. <https://doi.org/10.15784/601239>
- 585 Steig, Eric J., Jones, T. R., Schauer, A. J., Kahle, E. C., Morris, V. A., Vaughn, B. H., et al. (2021).  
586 Continuous-Flow Analysis of  $\delta^{17}\text{O}$ ,  $\delta^{18}\text{O}$ , and  $\delta\text{D}$  of  $\text{H}_2\text{O}$  on an Ice Core from the South  
587 Pole. *Frontiers of Earth Science in China*, 9, 72. <https://doi.org/10.3389/feart.2021.640292>
- 588 Stenni, B., Sarchilli, C., Masson-Delmotte, V., Schlosser, E., Ciardini, V., Dreossi, G., et al.  
589 (2016). Three-year monitoring of stable isotopes of precipitation at Concordia Station, East  
590 Antarctica. *The Cryosphere*, 10(5), 2415–2428. <https://doi.org/10.5194/tc-10-2415-2016>
- 591 Tarasov, L., Dyke, A. S., Neal, R. M., & Peltier, W. R. (2012). A data-calibrated distribution of  
592 deglacial chronologies for the North American ice complex from glaciological modeling.  
593 *Earth and Planetary Science Letters*, 315–316, 30–40.  
594 <https://doi.org/10.1016/j.epsl.2011.09.010>
- 595 Taylor, K. E., Williamson, D., & Zwiers, F. (2000). The sea surface temperature and sea-ice  
596 concentration boundary conditions for AMIP II simulations. Program for Climate Model  
597 Diagnosis and Intercomparison, Lawrence Livermore National Laboratory. Retrieved from  
598 <https://pcmdi.llnl.gov/report/pdf/60.pdf?id=16>
- 599 Toggweiler, J. R., Russell, J. L., & Carson, S. R. (2006). Midlatitude westerlies, atmospheric  $\text{CO}_2$ ,  
600 and climate change during the ice ages. *Paleoceanography*, 21(2).  
601 <https://doi.org/10.1029/2005PA001154>
- 602 Tremaine, D. M., Froelich, P. N., & Wang, Y. (2011). Speleothem calcite formed in situ: Modern  
603 calibration of  $\delta^{18}\text{O}$  and  $\delta^{13}\text{C}$  paleoclimate proxies in a continuously-monitored natural

- 604 cave system. *Geochimica et Cosmochimica Acta*, 75(17), 4929–4950.  
605 <https://doi.org/10.1016/j.gca.2011.06.005>
- 606 Turner, J., Phillips, T., Thamban, M., Rahaman, W., Marshall, G. J., Wille, J. D., et al. (2019). The  
607 dominant role of extreme precipitation events in antarctic snowfall variability. *Geophysical  
608 Research Letters*, 46(6), 3502–3511. <https://doi.org/10.1029/2018gl081517>
- 609 Uemura, R., Motoyama, H., Masson-Delmotte, V., Jouzel, J., Kawamura, K., Goto-Azuma, K., et  
610 al. (2018). Asynchrony between Antarctic temperature and CO<sub>2</sub> associated with obliquity  
611 over the past 720,000 years. *Nature Communications*, 9(1), 961.  
612 <https://doi.org/10.1038/s41467-018-03328-3>
- 613 Wang, S., Ding, M., Liu, G., Li, G., & Chen, W. (2023). Blocking Events in East Antarctica:  
614 Impact on Precipitation and Their Association with Large-scale Atmospheric Circulation  
615 Modes. *Journal of Climate*, 1(aop). <https://doi.org/10.1175/JCLI-D-23-0419.1>
- 616 Watanabe, M., Suzuki, T., O’ishi, R., Komuro, Y., Watanabe, S., Emori, S., et al. (2010).  
617 Improved Climate Simulation by MIROC5: Mean States, Variability, and Climate  
618 Sensitivity. *Journal of Climate*, 23(23), 6312–6335.  
619 <https://doi.org/10.1175/2010JCLI3679.1>
- 620 Werner, M., Jouzel, J., Masson-Delmotte, V., & Lohmann, G. (2018). Reconciling glacial  
621 Antarctic water stable isotopes with ice sheet topography and the isotopic  
622 paleothermometer. *Nature Communications*, 9(1), 3537. [https://doi.org/10.1038/s41467-  
623 018-05430-y](https://doi.org/10.1038/s41467-018-05430-y)
- 624 Wille, J. D., Favier, V., Gorodetskaya, I. V., Agosta, C., Kittel, C., Beeman, J. C., et al. (2021).  
625 Antarctic atmospheric river climatology and precipitation impacts. *Journal of Geophysical  
626 Research*, 126(8). <https://doi.org/10.1029/2020jd033788>